Pre-Compliance Test Method for Radiated Emissions with Multiple Segment Transfer Functions

D. Schneider [#1], M. Böttcher [#], S. Tenbohlen [#], W. Köhler [#]

[#] Institute of Power Transmission and High Voltage Technology (IEH)
University of Stuttgart
[1] daniel.schneider@ieh.uni-stuttgart.de

Abstract— **Radiated emission testing of electric components, modules and systems is mandatory. Such tests are performed during the development process. Due to strict time schedules and limited access to EMC measurement facilities, fast applicable pre-compliance methods are needed. Early knowledge of a product's EMC performance is indispensable for the developer to initiate required measures immediately. This is directly correlated to overall cost reduction. This paper deals with a pre-compliance test method for radiated emissions. The method is adapted to the CISPR 25 standard for automotive components and modules. Here, a setup is defined including equipment under test connected via a cable harness to a load. The site of operation is the developer's laboratory setup. Common mode currents on the cable harness are used to predict the radiated field strength occurring in an absorber-lined shielded enclosure. Therefore, multiple transfer functions are generated with a vector network analyzer in an absorber-lined shielded enclosure. Those transfer functions represent the correlation between common mode current segments in the defined test setup environment and their electric field strengths. Current probe measurements outside a test chamber along the cable harness of the equipment under test in combination with those transfer functions lead to a prediction of the radiated emissions. The multiple segment transfer functions method will be described and applied to practical real test setups.**

Keywords - CISPR 25; EMC; Pre-Compliance Test; Radiated Emission; Transfer Functions

I. Introduction

Electric components require radiated emission tests. EMC measurements are carried out according to CISPR 25 [1] for the automotive area. Those measurements take place in absorber-lined shielded enclosures (ALSE). The test setup is situated on a grounded metallic table bonded to the enclosure. It consists of the equipment under test (EUT), its cable harness, a load, optionally line impedance stabilization networks (LISNs), and a power supply. A measurement antenna is arranged one meter in front of the setup.

EMC engineering in parallel to the development process is very challenging due to strict time schedules and limited access to EMC measurement facilities. From the equipment manufacturer's point of view, an early knowledge of the EMC performance is important regarding suitable counter measures. Pre-compliance test methods with no need of an ALSE can fulfill the requirements of being on-site, fast and low-cost.

Apart from CISPR 25 measurements and complex simulations, methods predicting radiated emissions have been investigated. They mainly use the field domination of common mode currents on a harness [2]. This permits current probe measurements along a cable bundle as the basis for calculating radiated emissions.

Analytical methods which rely on the Hertzian dipoles model representing a cable harness and considering the geometry of the test setup are investigated in [3], [4], [5], and recently in [6]. A hybrid approach employing multiple measured transfer functions (TF) and computed phase information was presented in [7]. This approach uses TFs of cable harness segments along the harness' position. Hence, the method includes the entire measurement environment, such as the anechoic chamber characteristics, near field coupling of the measurement antenna with the setup and the geometrical conditions. Implementing this environment into a numerical or analytical model is extremely difficult and not constructive regarding pre-compliance, time consumption and effectiveness. A less complex adaption of the TF method with a faster procedure using scattering parameters measured with a vector network analyzer (VNA) was analyzed in [8]. Here, only a single TF was used. The single segment approach is limited to similar setups due to changing current distributions on cable harnesses for different setups and EUTs. An advanced version of [7] will be investigated for a more flexible method.

Section II presents the principle methodology of TFs, followed by section III explaining the current distribution along a cable harness needed for calculation. Section IV points out the multiple segment transfer functions (MSTF) method and its theoretical background. The verification and the usability of this advanced method are shown in section V and VI. A battery-driven impulse generator and a wiper motor are analyzed as the EUTs.

II. Methodology of Transfer Functions

The TF method uses a measurement procedure to obtain the correlation between current and electric field strength, similar to the formulas used in analytical models. More precisely, the common mode current on a cable harness and the radiated field are set in relation to each other. The contribution of differential mode currents to the entire field strength is neglected due to the closely spaced geometry of harness [2], [8]. This method contains properties of the test setup which are difficult to describe by formulas, e.g. near field coupling of the antenna with the setup, anechoic chamber characteristics, and the geometrical conditions of the entire setup. This is achieved by the use of a current probe detecting the common mode current $I_{CM}(f)$ on a harness and by an antenna measuring the electric field strength $E(f)$ in an ALSE. The TF in the frequency domain for an entire cable harness representing a single segment, as in Fig. 1, is defined by:

$$\boldsymbol{TF(f)} = \frac{\boldsymbol{E(f)}}{\boldsymbol{I_{CM}(f)}} \tag{1}$$

The generation of a TF using a VNA is presented in [8]. Here, a TF is generated for one defined test setup, as a first step. For this purpose, the VNA is connected to the test setup as depicted in Fig. 1 leading to $TF(f)$:

$$\boldsymbol{TF(f)} = \left|\frac{\boldsymbol{S_{31}(f)}}{\boldsymbol{S_{21}(f)}}\right| \cdot \boldsymbol{AF(f)} \cdot \boldsymbol{Z_T(f)} \tag{2}$$

with the scattering parameters S_{31} and S_{21}, the antenna factor AF and the transimpedance Z_T of the current probe.

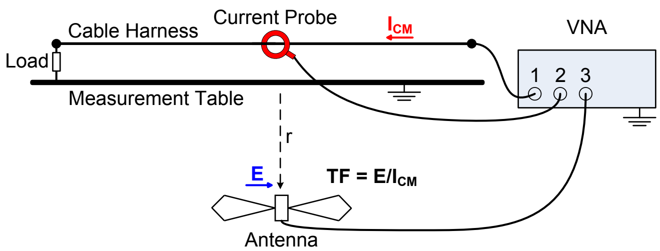

Fig. 1: Measurement setup for a single segment TF

As a second step, a current probe measurement with an EMI test receiver on a test setup with an EUT of interest follows. This setup is located at the developer's laboratory. The EUT is connected to the cable harness instead of the VNA. The common mode current $I_{EUT}(f)$ measured on the same position as during the TF generation and the according $TF(f)$ lead to the calculated electrical field strength $E_{pred}(f)$ representing the predicted pre-compliance result of radiated emission:

$$\boldsymbol{E_{pred}(f)} = \boldsymbol{TF(f)} \cdot \boldsymbol{I_{EUT}(f)} \tag{3}$$

Due to the nature of the method, a TF includes the common mode current distribution on the cable harness in combination with the VNA. A precondition for the single segment approach including only one current probe measurement is an identical current distribution for the EUT setup and the TF generation setup. Changed current amplitudes are regarded by the linear behavior of current and electric field. The change from VNA to an arbitrary EUT can affect the method based on changed parasitic capacitances and load impedances. The same applies if there is a difference between the setup in an ALSE and the corresponding laboratory setup. Hence, the pre-compliance result can be corrupted. The single segment TF is to be used product-specific or for similar setups [8]. A more flexible but elaborate attempt is presented in [7] employing multiple TFs representing a segmented cable harness. The MSTF, an advanced approach, will be discussed below.

III. Current Distribution

The overall current distribution on a cable bundle has to be known for a proper estimation of the electric field radiated from a harness. This is required for a calculation model as well as for a multiple segment method. The overall common mode current envelopes for each frequency point can be obtained by multiple current probe measurements with an EMI test receiver in peak mode along a harness. The question is: Which current distribution leads to the peak value of the electric field strength? Those measured envelopes do not have to be the current distributions for the corresponding peak value of the electric field strength measured by an antenna. This is only the fact if there is a standing wave on the cable. Envelopes can be used for frequencies where the cable is electrically small. Otherwise, they are an approximation.

Mostly, there are propagating composite waves consisting of forward and reflected waves with a current standing wave ratio (CSWR) smaller than infinite. Hence, an infinite series of distribution curves for each frequency exists. Only one of them per frequency is correlated to the measured peak value of the electric field. For the far field, it is the one with the highest surface integral. Under near field conditions, it is assumed to behave identically. Fig. 2 shows a calculated and theoretical series of 36 distribution curves for 200 MHz, their maximum and minimum envelopes and the distribution $I_{composite}$ with the highest surface integral. The series of curves are equally spaced with a phase shift of $2\pi/10$. The length of the cable is 1.75 m, the CSWR equals two, and cable attenuation is 0 dB.

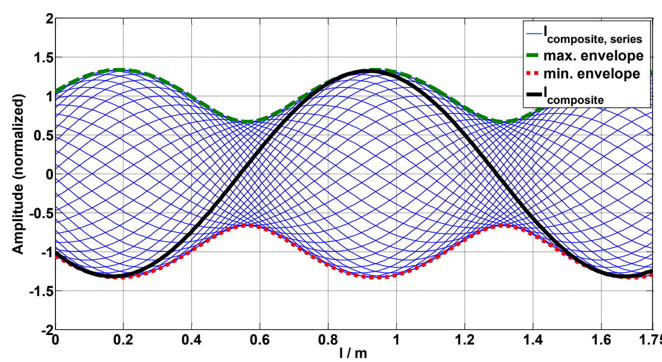

Fig. 2: Calculated current distribution at 200 MHz for a 1.75 m long cable

It is possible to retrieve a series of distribution curves out of a measured envelope. This is suitable as long as the cable length is bigger than half the wave length of the frequency of interest. In this case, at least one maximum and one minimum is contained. For shorter cable lengths, it is still a proper approximation. This allows the calculation of forward waves, reflected waves and their composites. Fig. 3 shows a measurement result of a 1.75 m long two-wire cable harness at 200 MHz excited by a VNA. Seven current probe measurements are taken, each 0.25 m, starting at the sample position 0.125 m. The current distribution $\hat{I}$ can be calculated out of the envelope and phase shift information. The computation of the composite $I_{composite}$ with maximum surface integral is more precise. Both types of current distribution will be used in the following. This example already shows the difference between $\hat{I}$ and $I_{composite}$. Assuming that $I_{composite}$ is the correct current distribution for the maximum field, an error in the field calculation using $\hat{I}$ will occur.

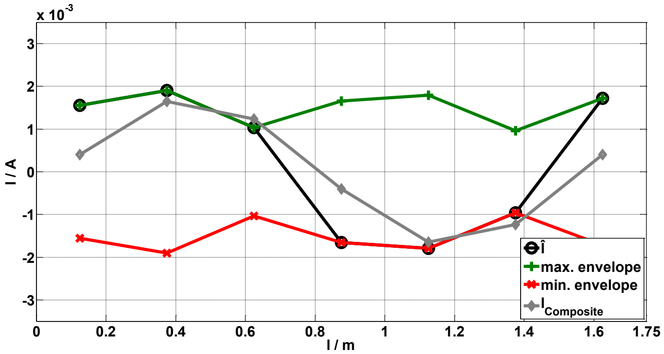

Fig. 3: Current distribution at 200 MHz for a 1.75 m two-wire cable out of 7 sampling points

Extra sampling points are inserted for a better reproduction of the current distribution. The separation distance is 0.125 m leading to 13 sampling points. Fig. 4 shows smoother curve shapes for $\hat{I}$ *extra Points* and $I_{composite}$ *extra Points* than Fig. 3. $I_{composite}$ *extra Points* represents the best approximation of the current distribution.

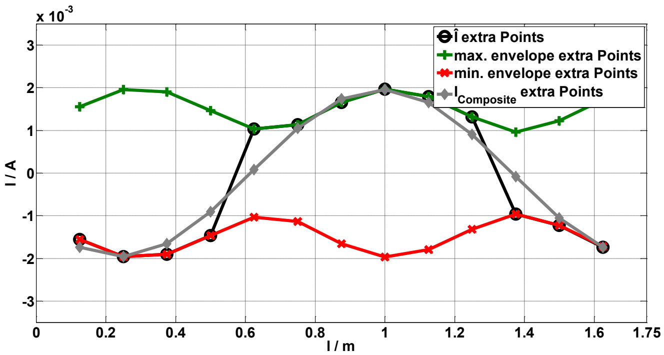

Fig. 4: Current distribution at 200 MHz for a 1.75 m two wire cable out of 13 sampling points

Fig. 5 shows $I_{composite}$ and $I_{composite}$ *extra Points* compared to the envelopes for 30 MHz. All current distributions presented give an accurate approximation for low frequencies.

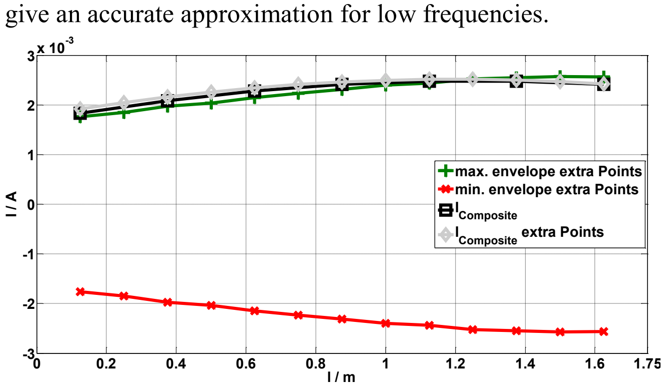

Fig. 5: Current distribution at 30 MHz for a 1.75 m two-wire cable out of 7 and 13 sampling points

IV. Multiple Segment Transfer Functions

The MSTF method is an adaption of the numerical computational Method of Moments (MoM) [9] in a measurement method. The starting point of the MoM is an electric field integral equation with a Green's function and a current distribution. A discretization of radiation sources into segments is carried out. For each segment, an approximation of the current with a basis function is computed, followed by the evaluation of the electric field.

For the MSTF, a cable harness representing the radiation source is divided into several segments. For each ith segment and its position as a field equation, a TF_i has to be generated according to (2). As in Fig. 6, a segment is moved to each position situated along the entire cable harness. The measurement setup is based on CISPR 25.

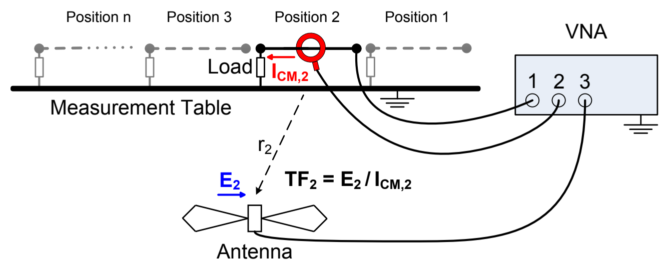

Fig. 6: Setup for the generation of multiple transfer functions

A segment consists of a part of the cable harness used later. Its length L should be electrically small compared to the wave length of the highest frequency of interest [5]. This is necessary to achieve a constant current distribution along the segment. This contribution focuses on a two-wire harness for plus and minus power supply, such as that used in the automotive area. Each wire has a common mode load Z_{CM} with the value of 260 Ω, its wave impedance against ground. Additionally, they have a differential mode termination Z_{DM} between each other of 390 Ω. Those terminations are applied for suppressing reflected waves and simulating the continuity of the cable harness segment. Fig. 7 shows a schematic of a segment and Fig. 8, the employed segment consisting of two 0.25 m long wires, a coupling printed circuit board (PCB), a termination PCB, and the attached current probe.

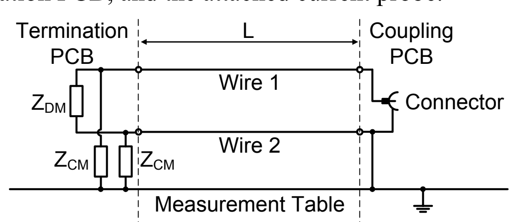

Fig. 7: Schematic of the segment for the transfer function generation

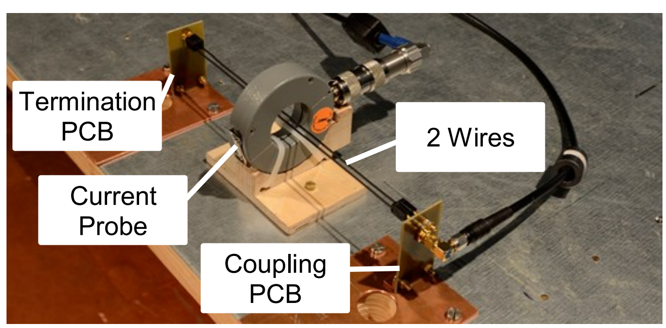

Fig. 8: Two-wire segment for the transfer function generation

Each segment has a distance r_i to the measurement antenna causing a phase shift. A TF set of scattering parameters includes the phase information between segment and antenna and is represented by the angle of S_{31}:

$$\boldsymbol{\varphi_{E,i} = \measuredangle S_{31,i}} \tag{4}$$

In addition to the phase information of the electric field, the phase shift of the current between the segments has to be known and taken into account. Hence, the entire cable harness has to be set up like in Fig. 1. The harness is excited by Port 1 of the VNA. Port 2 is connected to the current probe. For all positions a TF is generated for a S_{21} measurement with the probe around the harness has to be carried out. This leads to the phase information of the current for each segment:

$$\boldsymbol{\varphi_{I,i} = \measuredangle S_{21,i}} \tag{5}$$

A prediction of the electric field can be achieved with all the information of the single segments. Therefore, as a last step, current probe measurements on the EUT's test setup are needed at each position where a *TF* is available. The currents measured $I_{EUT,i}$ and the according TF_i lead to calculated electrical field strength E_{pred} by superposition, as shown in Fig. 9. The two current distributions $\hat{I}_{EUT}$ and $I_{EUT,composite}$ described in section III are taken into account by:

$$\boldsymbol{E_{pred,\hat{I}}(f) = \sum_{i=1}^{n} TF_i \cdot \hat{I}_{EUT,i}(f) e^{j\varphi_{I,i}(f)} e^{j\varphi_{E,i}(f)}} \tag{6}$$

$$\boldsymbol{E_{pred,Icomposite}(f) = \sum_{i=1}^{n} TF_i \cdot I_{EUT,composite,i}(f) e^{j\varphi_{E,i}(f)}} \tag{7}$$

By using $I_{EUT,composite}$ measured phase information $\varphi_{I,i}$ is not necessary.

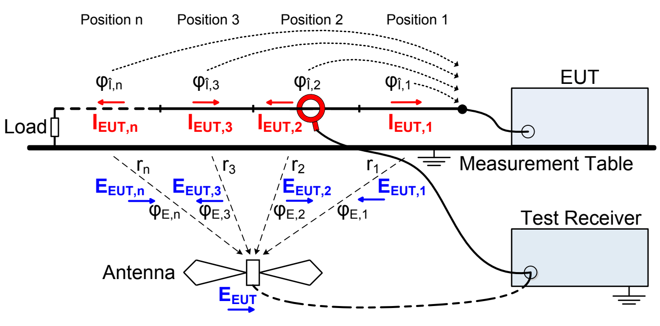

Fig. 9: Calculation of E_{EUT} by superposition of each segment's field fraction

V. Verification of the MSTF

Predicted and measured electric field strength using the same noise source have to be compared to check the quality of the MSTF. The test setup consists of a 1.75 m long two-wire harness and is located 50 mm above a ground plane corresponding to CISPR 25. It is terminated with its wave impedance as a segment in section IV. The setup is excited by a VNA acting as a broadband source, shown in Fig. 10. TF and phase data of this setup are gained as described in section IV. The common mode currents $I_{CM,i}$ are measured using an EMI test receiver at the same locations TF_i and phase data are determined. Variations in ground potential of the VNA and EMI test receiver can affect the accuracy of the method. Therefore, the VNA and EMI test receiver are located on the same ground plane. The predicted electric field strength caused by the excited harness can be calculated by (6) and (7). For comparison, the electric field strength is measured using a horizontally polarized biconical antenna connected to the EMI test receiver. The test setup remains the same as described above. The noise floor of the EMI test receiver and the VNA is more than 40 dB below the emission of the harness. Concerning the VNA and EMI test receiver, the frequency step size is 0.5 MHz in a range of the available antenna factor from 30 to 210 MHz. The intermediate frequency bandwidth is 120 kHz for the EMI test receiver and 500 Hz for obtaining TFs and phase data by the VNA. Currents and electric field strength are measured in peak mode for every frequency step.

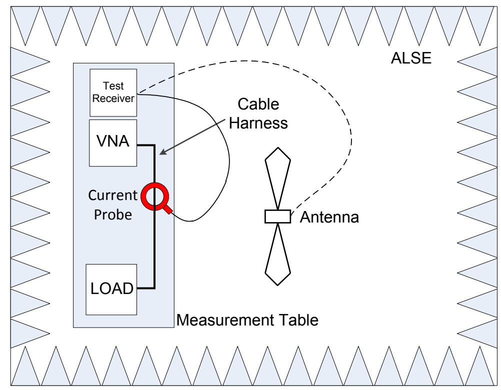

Fig. 10: Test setup for verification purposes in an ALSE

The comparison between the measured and by calculation predicted electric field strengths, $E_{meas,\ VNA}$, respectively $E_{pred,\ VNA}$ *with* $\hat{I}$ and $E_{pred,\ VNA}$ *with* $I_{composite}$, is shown in Fig. 11. It shows that $E_{meas,\ VNA}$ and $E_{pred,\ VNA}$ *with* $\hat{I}$ correlate within a frequency range of 35 to 121 MHz and 173 to 210 MHz with a maximum tolerance of 5 dB. $E_{pred,\ VNA}$ *with* $I_{composite}$ which is computed by a series of 720 current distribution curves with a phase shift of 2π/720 replicates $E_{meas,\ VNA}$ with a maximum offset of 8 dB in the named frequency range. The λ resonance frequency at 169 MHz of the harness which occurs in $E_{meas,\ VNA}$ is moved to 160 MHz in $E_{pred,\ VNA}$ *with* $\hat{I}$ and to 174.5 MHz in $E_{pred,\ VNA}$ *with* $I_{composite}$. A potential reason for the differences around 170 MHz is the number of locations and the related length of segments on which TFs, phase data and currents are obtained. Resonance frequencies are sensitive concerning discretization and difficult to replicate. With a segmentation of seven concerning the 1.75 m long cable harness, the electrical length of a segment is λ/6.75 at the resonance frequency of 169 MHz. For better correlation at resonance, a shorter electrical length of a segment is needed.

In Fig. 12, the field prediction calculation is extended by six additional locations so that the length of a segment is reduced to 0.125 m. To avoid effort, extra phase data and TFs are generated by calculating the average of two adjacent TFs and phase data sets. Additionally, a correction factor taking shorter segments into account is introduced. The additional current data is measured by an EMI test receiver. By increasing the number of sampling points, the tolerance of the correlation between $E_{meas,\ VNA}$ and $E_{pred,\ VNA}$ *with* $\hat{I}$*, extra Points*, respectively $E_{pred,\ VNA}$ *with* $I_{composite}$*, extra Points* is reduced to about 4 dB within the whole frequency range of 30 to

210 MHz, neglecting differences of maximum 8 dB at certain frequency ranges around 140 and 170 MHz. Calculation with $I_{composite}$, *extra Points* results in better correlation, especially for higher frequencies.

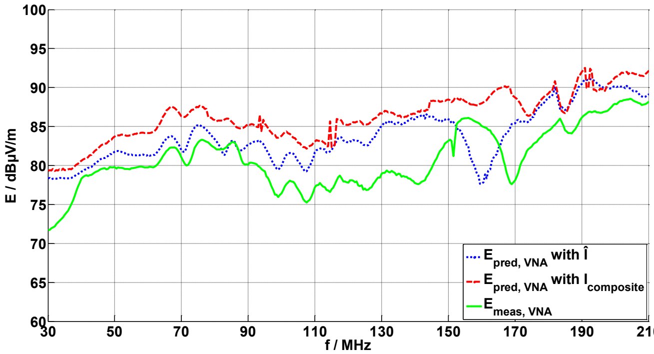

Fig. 11: Verification result of the MSTF for seven sampling points

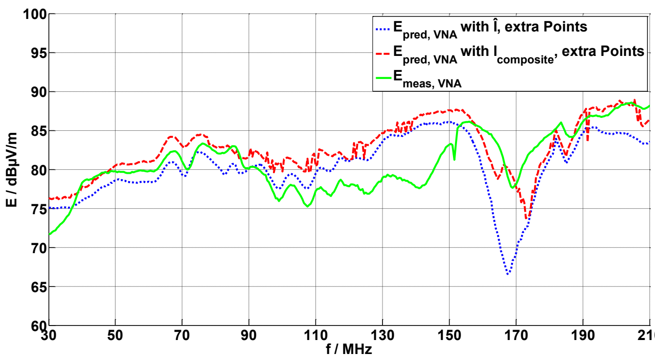

Fig. 12: Verification result of the MSTF for 13 sampling points

As a result, the prediction of the electric field using the methodology of the MSTF is proven. Adequate accuracy within ± 4 dB (neglecting cable resonance frequencies) can be achieved by the use of 13 sampling points for the current distribution. Deviations between field prediction and measurement are caused by multiple reasons: radiation, phase stability and position of the measurement cables, feedback of the current probe during TFs generation and measuring current, the current distribution, influence of a segment during the TF generation, imperfect termination impedances, and geometrical and measurement uncertainties. A determination of the overall uncertainty has to be performed in the future

VI. Investigation of Use Cases

A battery-driven broadband impulse generator from Schwarzbeck (SB), is used as the noise source to prove the applicability of the MSTF. The SB shares the same ground potential as the EMI test receiver, see Fig. 13. The test setup remains the same as described above. The TFs and phase data obtained in section V are used for computing the electric field strength. The currents ICM,i are measured every 0.125 m giving the possibility of having either 7 or 13 sampling points. The electric field strength is measured with an EMI test receiver for comparison.

The predicted electric field strengths $E_{pred,\,SB}$ *with* $\hat{I}$ and $E_{pred,\,SB}$ *with* $I_{composite}$ are compared in Fig. 14 with the measured electric field strength $E_{meas,\,SB}$. As can be seen, the deviation between field measurement and prediction is mostly below 5 dB, neglecting the λ resonance of the cable harness, which is at 170 MHz. The resonance is moved to 159.5 MHz in $E_{pred,\,SB}$ *with* $\hat{I}$ and 174 MHz in $E_{pred,\,SB}$ *with* $I_{composite}$, respectively, due to the number of locations on which TFs, phase data and currents are obtained, as described in section V.

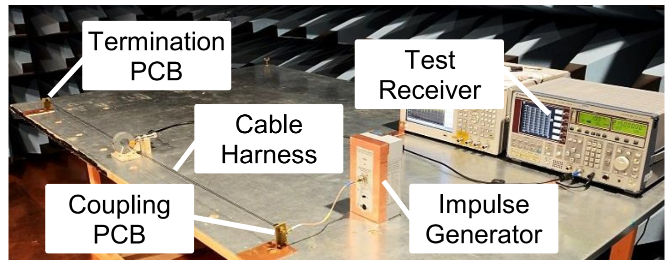

Fig. 13: Test setup for the impulse generator Schwarzbeck IGUF 2910 S

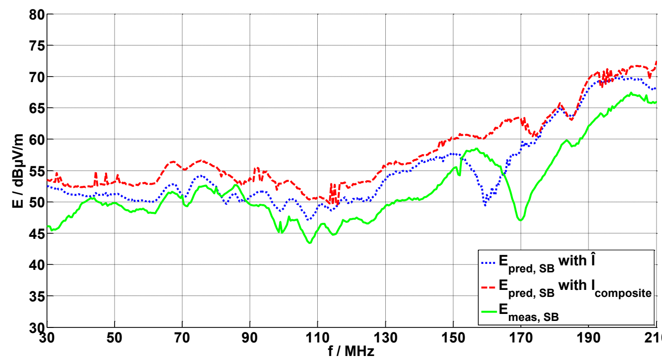

Fig. 14: Prediction result for the impulse generator SB for 7 sampling points

Extra sampling points are introduced reducing the length of a segment to 0.125 m in the same way as for the verification. Therefore, the computation of the electric field strength is more accurate. As can be seen in Fig. 15, the resonance frequency of the cable harness at 170 MHz is nearly replicated by $E_{pred,\,SB}$ *with* $I_{composite}$, *extra Points* with a maximum deviation of 7 dB. Overall, mainly less than 3 dB of deviation occurs. $E_{pred,\,SB}$ *with* $\hat{I}$, *extra Points* also delivers a good prediction, except in the region of the cable resonance.

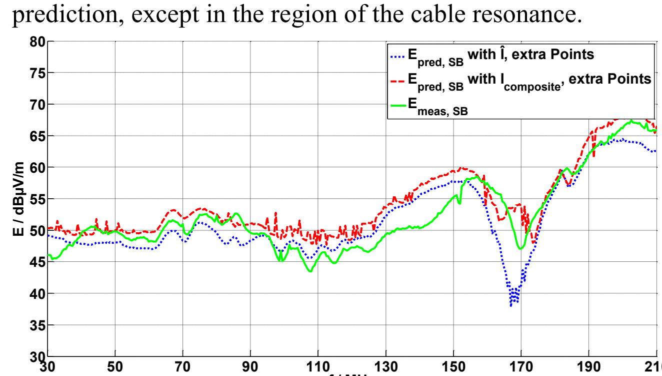

Fig. 15: Prediction result for the impulse generator SB for 13 sampling points

A realistic test setup corresponding to CISPR 25 is used in the following. A wiper motor as the EUT is connected to a 1.75 m long two-wire harness and terminated with two LISNs, see Fig. 16. The harness is located 50 mm above the ground plane and a 12 V car battery is connected to the LISNs. The EMI test receiver shares the same ground potential as the LISNs and the negative terminal of the battery. A new TF is generated for the last segment from 1.5 to 1.75 m using the LISNs as termination instead of the wave impedance termination PCB. The rest of the TFs are determined as described in section IV. As termination of the harness when measuring the currents, the electric field strength and phase data the LISNs are used instead of the termination PCB. The currents $I_{CM,i}$ are measured again each 0.125 m giving the possibility of having either 7 or 13 sampling points. For comparison, the electric field strength is measured with an EMI test receiver.

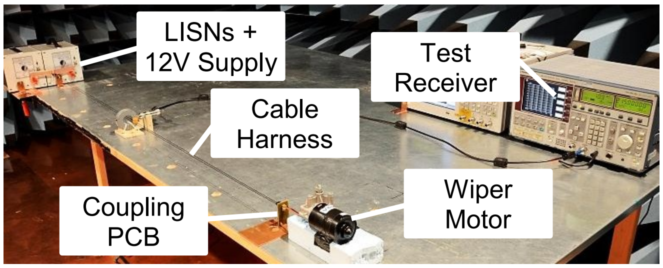

Fig. 16: Test setup for a wiper motor supplied over LISNs

The prediction and measurement of the electric field strength using 13 sampling points is shown in Fig. 17. As can be seen, the deviation between $E_{pred,\ Motor}$ *with* $\hat{I}$, *extra Points*, $E_{pred,\ Motor}$ *with* $I_{composite}$, *extra Points* and $E_{meas,\ Motor}$ is partially better than 10 dB for a frequency range of 30 to 68 MHz, 90 to 115 MHz and 176 to 210 MHz. The differences in correlation result in the TFs used comprising the termination PCB. In future work, the impedance of the LISNs has to be transformed to each location of the termination PCB of a segment instead of a fixed value that equals the wave impedance of the cable harness.

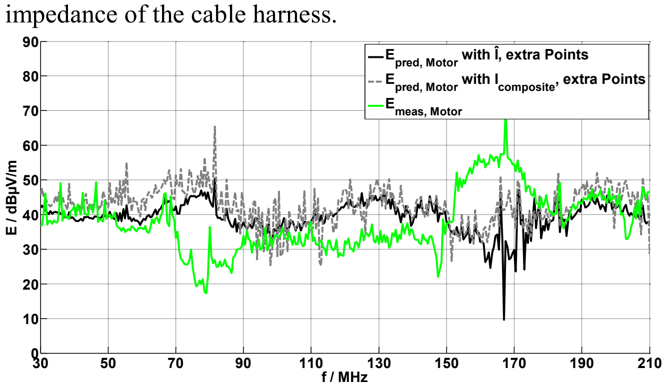

Fig. 17: Prediction result for the wiper motor with 13 sampling points

VII. Conclusion and Outlook

This paper presents an advanced method for the prediction of radiated emissions. The measurement setups used are according to the CISPR 25 standard for component tests. This method can be applied to other standards as well. Multiple current probe measurements on an EUT's cable harness in combination with appropriate TFs lead to a fast estimation of radiated emissions under the premise of field dominating common mode currents on a cable harness. This pre-compliance method can be applied to a developer's laboratory setup without having an ALSE. Thus, this method can be easily integrated into a component's development process.

The methodology and the verification of the MSTF method is elucidated and current distribution as a basis is explained. An impulse generator and a wiper motor setup proof the applicability. The estimation of the impulse generator's emissions is mainly better than 3 dB using a sufficient number of sampling points. Cable resonances are identified as critical. Regarding the wiper motor, an estimation mostly better than 10 dB is achieved. This reduced accuracy can be explained by the TFs applied not representing the LISNs perfectly.

Due to the potential of this pre-compliance method, there will be ongoing research. The frequency ranges from 0.15 to 200 MHz in vertical and horizontal polarizations have to be covered. As a result of the observed deviations between predicted and measured field strengths an uncertainty analysis of the whole method has to be carried out. A superior current distribution algorithm with the need for fewer measurements will reduce effort. Shorter segments during the TF generation can increase the accuracy of the pre-compliance test result. Furthermore, the method has to be expanded to multiple wire bundles and different grounding and load concepts.

References

[1] I. E. Comission, "CISPR 25 Ed.3: Vehicles, boats and internal combustion engines - Radio disturbance characteristics - Limits and methods of measurement for the protection of on-board receivers," 2008.

[2] C. R. Paul, "A comparison of the contributions of common-mode and differential-mode currents in radiated emissions," *Electromagnetic Compatibility, IEEE Transactions on*, vol. 31, no. 2, pp. 189-193, May 1989.

[3] Z. Desheng, C. W. Hoe, and L. C. Kin, "Modeling of radiated electromagnetic emission coming from interface cables of an equipment," *Electromagnetic Compatibility, 1996. Symposium Record. IEEE 1996 International Symposium on*, pp. 230-234, 1996.

[4] M. C. Di Piazza, A. Ragusa, G. Tine, and G. Vitale, "A model of electromagnetic radiated emissions for dual voltage automotive electrical systems," *Industrial Electronics, 2004 IEEE International Symposium on*, vol. 1, pp. 317-322, 2004.

[5] C. R. Paul, *Introduction to Electromagnetic Compatibility*. New York: John Wiley & Sons, Inc., 1992.

[6] J. Jia, D. Rinas, and S. Frei, "Prediction of radiated fields from cable bundles based on current distribution measurements," *Electromagnetic Compatibility (EMC EUROPE), 2012 International Symposium on*, pp. 1-7, Sep. 2012.

[7] W. T. Smith and R. K. Frazier, "Prediction of anechoic chamber radiated emissions measurements through use of empirically-derived transfer functions and laboratory common-mode current measurements," *Electromagnetic Compatibility, 1998. 1998 IEEE International Symposium on*, vol. 1, pp. 387-392, 1998.

[8] D. Schneider, S. Tenbohlen, and W. Köhler, "Pre-compliance test method for radiated emissions of automotive components using scattering parameter transfer functions," *Electromagnetic Compatibility (EMC EUROPE), 2012 International Symposium on*, pp. 1-6, Sep. 2012.

[9] F. M. Tesche, M. V. Ianoz, and T. Karlsson, *EMC Analysis Methods and Computational Models*. New York: John Wiley & Sons, Inc., 1997.